Auxiliary Material Submission for manuscript

"How is the ocean filled?"

Geoffrey Gebbie

Physical Oceanography Department, Woods Hole Oceanographic Institution

Peter Huybers

Department of Earth and Planetary Sciences, Harvard University

Contents

The total matrix intercomparison (TMI) method [*Gebbie and Huybers*, 2010] seeks the steady-state circulation that best fits modern-day tracer climatologies. The datasets include the WOCE tracer climatologies of temperature, salinity, phosphate, nitrate, and oxygen [*Gouretski and Koltermann*, 2004], as well as the GISS oxygen-18/oxygen-16 isotope ratio climatology [*Legrande and Schmidt*, 2006]. The search for a steady-state circulation is formalized as the least-squares problem of minimizing a sum of squared misfits between estimated and observed tracer distributions,

$$\mathrm{J} = (\mathbf{E}\mathbf{x} - \mathbf{y})^T (\mathbf{E}\mathbf{x} - \mathbf{y}) + \mu^T \mathcal{F}[\mathbf{x}], \tag{1}$$

where $\mathbf{x}$ is the state vector, $\mathbf{y}$ contains a suite of tracer observations, $\mathbf{E}$ is a matrix that maps the state vector onto the observations, T is the matrix transpose, μ is a Lagrange multiplier vector, and $\mathcal{F}[\mathbf{x}] = 0$ is the steady-state circulation constraint. The Lagrange multiplier term enforces the steady-state circulation requirement. Similar formulations have been used in the past [*Schlitzer*, 2007].

1. The steady-state circulation

First, we show a novel way to formulate the steady-state constraint and to solve for the steady-state circulation. In steady-state, a conservative tracer concentration in an interior box must be a linear combination of the tracer concentrations in neighboring boxes:

$$c_o = \sum_{i=1}^{6} m_i c_i \tag{2}$$

where the summation goes to 6 because there are 6 neighbors in three dimensions, and m_i is the volume (or nearly equivalently, mass) fraction from each neighboring box. In the case that a tracer is nonconservative, a source term must be added to the right hand side. This tracer equation can be rearranged such that all the terms are on the left hand side and the equation is equal to zero. Appending one equation for each interior point, we arrive at the operator $\mathcal{F}[\mathbf{x}]$, where the state vector $\mathbf{x}$ now includes all of the tracer distributions and the m_i mass fraction values.

The operator $\mathcal{F}$ is highly nonlinear as the state vector unknowns multiply each other. If we linearize about the observed tracer values, which is possible because we have complete gridded datasets for the tracers, then it is possible to solve for the mass fraction values between all interior boxes. To solve this subproblem, we have a non-negative least squares problem at every interior location, and it is set up so that there are seven constraints (tracer conservation equations plus mass conservation) and, at most, seven unknowns (6 mass fractions plus a nonconservative source term). The local sub-problem appears to be mathematically well-posed. In practice, some tracer information may not be independent, and thus we use a tapered and weighted least squares method to seek the the circulation with the minimum amount of diapycnal mixing that still fits the observations. The additional constraint is specified as a tapering of the least-squares solution, where the strength of the tapering is determined by the signal-to-noise ratio in the tracer observations [*Hansen*, 1992]. This approach regularizes the TMI matrix to produce a unique solution for the global pathways and guards against overfitting noise in the observations.

Putting all of the m_i values together, we form a linearized steady-state matrix, $\mathbf{F}$.

Multiplying the matrix by a vectorized tracer distribution, **Fc**, gives the imbalance from steady-state. If we append surface boundary conditions to **F**, we obtain the TMI pathways matrix **A**, discussed in Gebbie & Huybers (2010). Obtaining **A** is the first step of a 2-step inversion process.

There are a number of intricacies in finding **A** successfully. First, provisions must be made along the seafloor to connect broken or unresolved property tongues owing to the small spatial scales of dense water overflows, mid-ocean fracture zones, and episodic property transport. In particular, bottom flow is parameterized for those boxes poorly described by their immediate neighbors by searching over successively larger bottom areas for potential sources, beginning with a 2° radius and then incrementally increasing up to 16°, which we will show is sufficient to describe all bottom points in the datasets employed here.

Second, the ocean is not in a strict steady state. To minimize the influence of seasonality, we apply TMI to observations that represent late wintertime conditions by requiring that the ocean be well-mixed above the seasonally-maximum mixed-layer depth, reflecting the fact that this depth is most indicative of the properties transmitted into the ocean interior [*Stommel*, 1979]. Here we use the properties found at the base of seasonal mixed layer in order to define the *surface* properties that get transmitted into the ocean interior [*Stommel*, 1979]. A further issue is that disequilibrium between the surface and deep ocean is expected due to both natural ocean-atmosphere variability and anthropogenic changes [*Johnson and Orsi*, 1997; *Huang et al.*, 2003; *Curry and Mauritzen*, 2005; *Levitus et al.*, 2005; *Jacobs*, 2006; *Gouretski and Koltermann*, 2007]. Water-mass properties have changed in time [*Yashayaev and Clarke*, 2008], suggesting that TMI may not follow property tongues to their exact surface origin, but

the properties of different ocean basins are far more distinct than any observed changes in the instrumental record, suggesting that the solution will not be strongly biased. We proceed with the steady-state assumption as a provisional first-order description of the ocean, subject to posterior checks of the extent that non-steady behavior has distorted the solution.

The surface boundary conditions must be interpreted correctly. Note that contact with the atmosphere does not necessarily imply complete equilibration of a water type with overlying atmospheric conditions so that water properties may be indicative of exchanges at multiple locations, though for purposes of specificity we focus on the most recent exchange.

2. Estimating tracer distributions

It is necessary to determine if the global cost function has been sufficiently minimized. To determine whether the steady-state pathways are consistent with the tracer climatologies, we formulate a subset of the global cost function for each tracer type:

$$\mathrm{J}_c = (\mathbf{Ec} - \mathbf{c}_{obs})^T (\mathbf{Ec} - \mathbf{c}_{obs}), \tag{3}$$

where $\mathbf{c}$ is a vectorized tracer distribution with observations $\mathbf{c}_{obs}$, and all tracers have been rendered independent by the linearization step above. The computation of J_c, however, involves uncertain surface boundary conditions. If changes to the surface boundary conditions are expressed as a control vector $\mathbf{u}$, the steady-state circulation can be represented as:

$$\mathbf{Ac} = \mathbf{d} + \Gamma\mathbf{u}, \tag{4}$$

where $\mathbf{d}$ is a vector that contains the surface boundary conditions and interior sources and sinks and Γ is a matrix that maps the control vector into the proper parts of $\mathbf{d}$.

Inverting equation (4) and substituting into (3), we have:

$$\mathrm{J}_c = (\mathbf{E}\mathbf{A}^{-1}\mathbf{d} + \mathbf{E}\mathbf{A}^{-1}\Gamma\mathbf{u} - \mathbf{c}_{obs})^T(\mathbf{E}\mathbf{A}^{-1}\mathbf{d} + \mathbf{E}\mathbf{A}^{-1}\Gamma\mathbf{u} - \mathbf{c}_{obs}). \quad (5)$$

We can redefine the terms and write J solely as a function of **u**:

$$\mathrm{J}_c = \mathbf{u}^T\mathbf{H}\mathbf{u} + 2\mathbf{f}^T\mathbf{u} + \mathbf{r}^T\mathbf{r}, \quad (6)$$

where

$$\mathbf{H} = \Gamma^T\mathbf{A}^{-T}\mathbf{E}^T\mathbf{E}\mathbf{A}^{-1}\Gamma, \;\; \mathbf{f}^T = \Gamma^T\mathbf{A}^{-T}\mathbf{E}^T\mathbf{r}, \;\; \mathbf{r} = \mathbf{E}\mathbf{A}^{-1}\mathbf{d} - \mathbf{c}_{obs}. \quad (7)$$

Taking the partial derivative of J_c with respect to **u** and setting to zero, we can solve for the **u**, and hence **c**, that best fits the data:

$$\mathbf{u} = -\mathbf{H}^{-1}\mathbf{f}. \quad (8)$$

A first test is to see whether the estimated temperature, salinity, δ^{18}O, phosphate, nitrate, and oxygen fields are within their expected observational tolerances. In this case, the **E** matrix above is replaced with the identity matrix because we have complete gridded datasets. We find that all of the tracers are estimated within the published error estimates. After normalizing to make the expected J value for each tracer to be 1, we find that J equals 0.34 for temperature, 1.46 for salinity, 0.02 for δ^{18}O, 0.32 for phosphate, 0.67 for nitrate, and 1.22 for oxygen (see Fig. S1). The δ^{18}O dataset provides a rather weak constraint because of the large published errors relative to the water-mass signal [*Legrande and Schmidt*, 2006]. The actual error in δ^{18}O is probably smaller than we have used, so the overfitting of the data is not as bad as the J value makes it appear.

The TMI method allows the estimation of tracer distributions which were not used to obtain the **A** matrix, such as δ^{13}C. The use of withheld data to check the estimated steady-state

pathways represents a more stringent test, obviously. In this case, $\mathbf{E}$ transfers the δ^{13}C vector $\mathbf{c}$ from the WOCE hydrographic climatology grid onto the locations of the withheld data, $\mathbf{c}_{obs}$. Figure 1 of the main manuscript shows the results of this test, where the standard deviation of the misfit between estimated and observed carbon-13/carbon-12 isotope ratio is 0.2 per mil, an acceptable value.

3. Diagnosing water-mass pathways

If $\mathbf{c}$ is set to one in a surface patch of interest and zero elsewhere, the global distribution of the tracer $\mathbf{c}$ is found by inverting $\mathbf{A}$, i.e., $\mathbf{c} = \mathbf{A}^{-1}\mathbf{d}$. In practice, $\mathbf{A}^{-1}$ is not explicitly computed, but an LU factorization is used to calculate the product of $\mathbf{A}^{-1}$ and any vector. The resulting tracer distribution indicates the fraction of mass that has originated from that surface location [*Khatiwala et al.*, 2001; *Haine and Hall*, 2002].

The ability to accurately distinguish waters originating from nearby regions can be assessed by comparing the 2^o and 4^o resolution solutions. We find that the total amount of volume originating from the regional patches defined by Gebbie and Huybers (2010) is similar to within 2% between the two solutions, with the only exception being the ratio of Ross to Weddell Sea Waters. While the total amount of Antarctic Water is the same in both solutions, 36% of the global total, the breakdown of Weddell to Ross Sea Waters is different. In the 2° solution, Ross Sea Water is the origin of 20% of the global volume, but the 4° solution indicates that the Ross Sea is the origin of just 14% of global volume. In general, we find that zonal averages are insensitive to the resolution of the datasets.

4. Adjoint method for the surface origination map

Following the diagnosis of a water-mass pathway, the total volume of the interior ocean originating from a given surface box is then calculable as the sum of the volume of each box multiplied by the mass fraction dye tracer **c**:

$$V = \mathbf{v}^T \mathbf{c}, \tag{9}$$

where **v** is a vector of the volumes of each grid box. To make a global map of the amount of ocean volume originating from each location, one needs to calculate a complete **c** distribution for each of the 11,113 surface locations.

Substituting the value of **c** from the forward model equation, i.e., $\mathbf{c} = \mathbf{A}^{-1}\mathbf{d}$ into (9), we get:

$$V = \mathbf{v}^T \mathbf{A}^{-1} \mathbf{d}. \tag{10}$$

Now the sensitivity of V to changes in the boundary conditions can be solved with one inversion of the transpose of **A**:

$$\frac{\partial V}{\partial \mathbf{d}} = \mathbf{A}^{-T} \mathbf{v}, \tag{11}$$

where $-T$ refers to the inverse transpose of the matrix and the partial derivative is equal to $\mathbf{V}_{tot}$ in the main text. The terms of the resulting sensitivity vector that correspond to the surface give the change in volume for a given change in the surface boundary condition. This is exactly a map of the volume of the global ocean that has originated from each of the surface locations. This equation can also be found by the method of Lagrange multipliers (or an *adjoint method*), whereby we also arrive at the inverse of the transpose **A** matrix being important. This equation can be solved in just one matrix-vector product, a more efficient means of obtaining sensitivity

information. This calculation is used to produce the results shown in Figure 2 of the main text.

5. The distribution of water masses and its sensitivity to spatial resolution and noise

The distribution of water masses is easily diagnosed by taking the elements of $\partial V/\partial \mathbf{d}$ above that correspond to surface locations, then sorting them by relative size. The distribution is computed by using both the WOCE hydrographic climatologies at 2° and 4° horizontal resolution. When the 2° distribution is downscaled to 4°, the results are very similar (Fig. S3), and it appears that the solution characteristics are not a strong function of resolution.

Figure 3 of the main manuscript finds a near '-1' power law in the distribution of surface contributions. A simple tracer advection-diffusion model of an overturning circulation suggests a possible explanation. The simple setup is two-dimensional in the -yz plane with 25×25 gridpoints. A simple streamfunction has all of the downwelling occurring along the boundary with upwelling occurring everywhere else. We find that the slope of power law is proportional to the Peclet number. In essence, the power law provides an estimate of the entrainment that occurs during the downwelling limb of the overturning circulation.

Two other robustness tests are worthy of note. In an experiment in which uncorrelated noise with the magnitude of observational error is added to the actual observations, the first step (local step) of the TMI method cannot find a viable steady-state circulation to explain the data in over 50% of the points. This is contrast to the observations without additional noise, where the local step can satisfy the observations without error in over 99% of locations. Even though most of the local inversions are further out of balance than acceptable (in the

noise-added case), we can nonetheless proceed to the second step of a global inversion. Here we find, after completing the second step, that the reconstructed tracer fields are little perturbed by the additional noise. Apparently, the global inversion is able to filter out much of the local noise. These results hold the further opportunity that we can likely identify how far out of balance the present ocean circulation is. We also note that the ocean climatologies have been extensively averaged, and this likely makes it easier for TMI to find a steady-state solution.

In a second test, we used synthetic tracer data produced by S. Khatiwala from a steady-state version of the MIT General Circulation Model [*Khatiwala et al.*, 2005], with a known water-mass distribution that was treated as the "truth". Applying the TMI method to the synthetic observations, we recovered the GCM-modeled water-mass decomposition with an error of less than 5% in the deep ocean, and not larger than 10% in the upper ocean. The results of these tests suggests that the TMI method is robust.

Acknowledgment. We thank an anonymous reviewer for simplifying the derivation of the adjoint calculation for surface origins.

References

Curry, R., and C. Mauritzen (2005), Dilution of the northern North Atlantic Ocean in recent decades, *Science*, *308*(5729), 1772–1774.

Gebbie, G., and P. Huybers (2010), Total matrix intercomparison: a method for resolving the geometry of water-mass pathways, *J. Phys. Oceanogr.*, *40*(8), 1710–1728.

Gouretski, V., and K. Koltermann (2004), WOCE Global Hydrographic Climatology, *Tech. Rep. 35*, Berichte des Bundesamtes für Seeschifffahrt und Hydrographie.

Gouretski, V., and K. P. Koltermann (2007), How much is the ocean really warming?, *Geophysical Research Letters*, *34*(1).

Haine, T. W. N., and T. M. Hall (2002), A generalized transport theory: Water-mass composition and age, *J. Phys. Oceanogr.*, *32*(6), 1932–1946.

Hansen, P. C. (1992), Analysis of discrete ill-posed problems by means of the L-curve, *Siam Review*, *34*(4), 561–580.

Huang, B., P. Stone, A. Sokolov, and I. Kamenkovich (2003), The Deep-Ocean Heat Uptake in Transient Climate Change, *Journal of Climate*, *16*(9), 1352–1363.

Jacobs, S. (2006), Observations of change in the Southern Ocean, *Philosophical Transactions of the Royal Society A: Mathematical, Physical and Engineering Sciences*, *364*(1844), 1657–1681.

Johnson, G. C., and A. H. Orsi (1997), Southwest Pacific Ocean water-mass changes between 1968/69 and 1990/91, *Journal of Climate*, *10*(2), 306–316.

Khatiwala, S., M. Visbeck, and P. Schlosser (2001), Age tracers in an ocean GCM, *Deep-Sea Research I*, *48*(6), 1423–1441.

Khatiwala, S., M. Visbeck, and M. A. Cane (2005), Accelerated simulation of passive tracers in ocean circulation models, *Ocean Modelling*, *9*(1), 51–69.

Legrande, A. N., and G. A. Schmidt (2006), Global gridded data set of the oxygen isotopic composition in seawater, *Geophysical Research Letters*, *33*(12).

Levitus, S., J. Antonov, and T. Boyer (2005), Warming of the world ocean, 1955-2003, *Geophysical Research Letters*, *32*(2).

Schlitzer, R. (2007), Assimilation of radiocarbon and chlorofluorocarbon data to constrain deep and bottom water transports in the world ocean, *Journal of Physical Oceanography*, *37*(2), 259–276.

Stommel, H. (1979), Determination of water mass properties of water pumped down from the Ekman layer to the geostrophic flow below, *Proc. Natl. Acad. Sci.*, *76*, 3051–3055.

Yashayaev, I., and A. Clarke (2008), Evolution of North Atlantic water masses inferred from Labrador Sea salinity series, *Oceanography*, *21*(1), 30–45.

Received _____

Figure 1.

Figure 2.

Figure 3.

Figure Captions

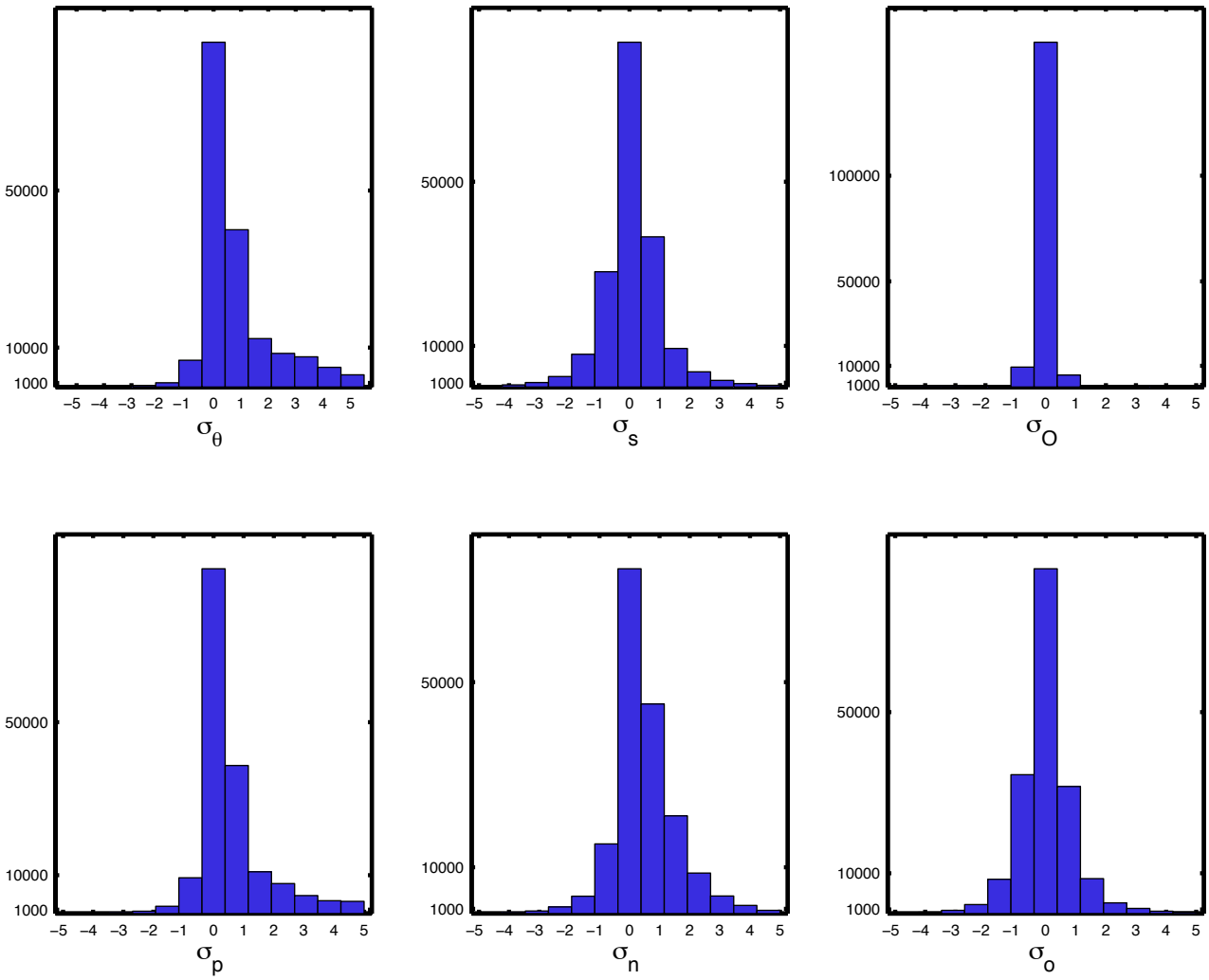

Figure 1. Histograms of the misfit between the TMI surface-boundary solution and observations for potential temperature (*top left*), salinity (*top middle*), $\delta^{18}O$ (*top right*), phosphate (*bottom left*), nitrate (*bottom middle*), and oxygen (*bottom right*). In all cases, the misfits have been divided by the published error in the climatological tracer fields and are reported in standard deviations.

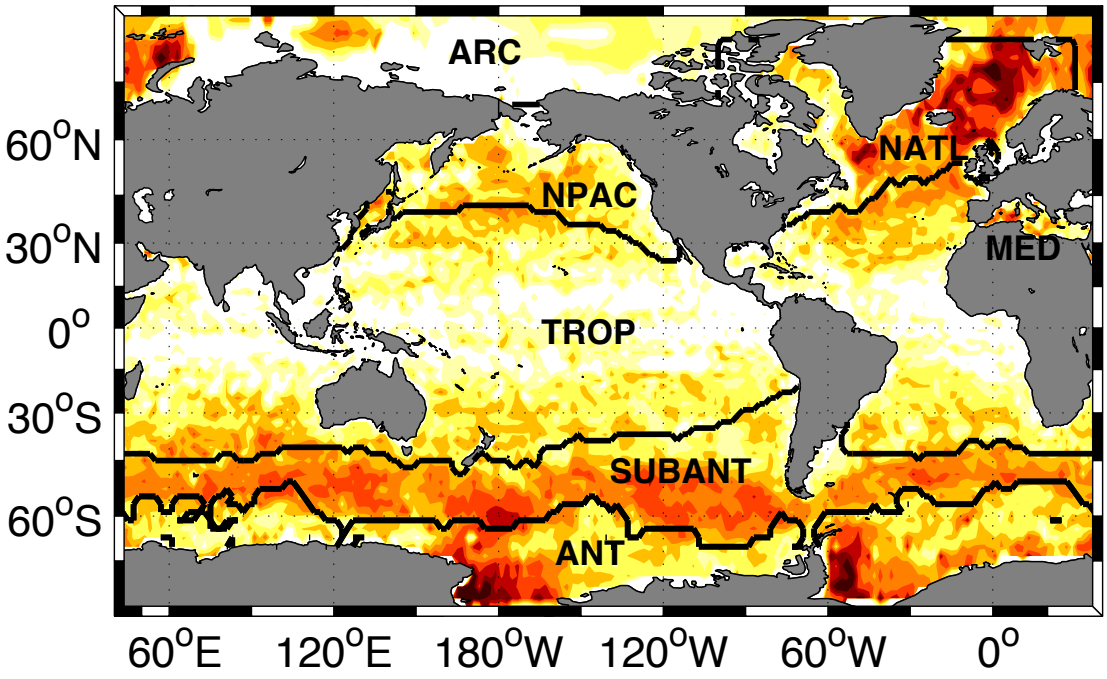

Figure 2. Ocean surface divided into seven surface regions (ANT = Antarctic Water, NATL = North Atlantic Water, SUBANT = Subantarctic Water, NPAC = North Pacific Water, ARC = Arctic Water, MED = Mediterranean Water, TROP = Tropical and subtropical waters).

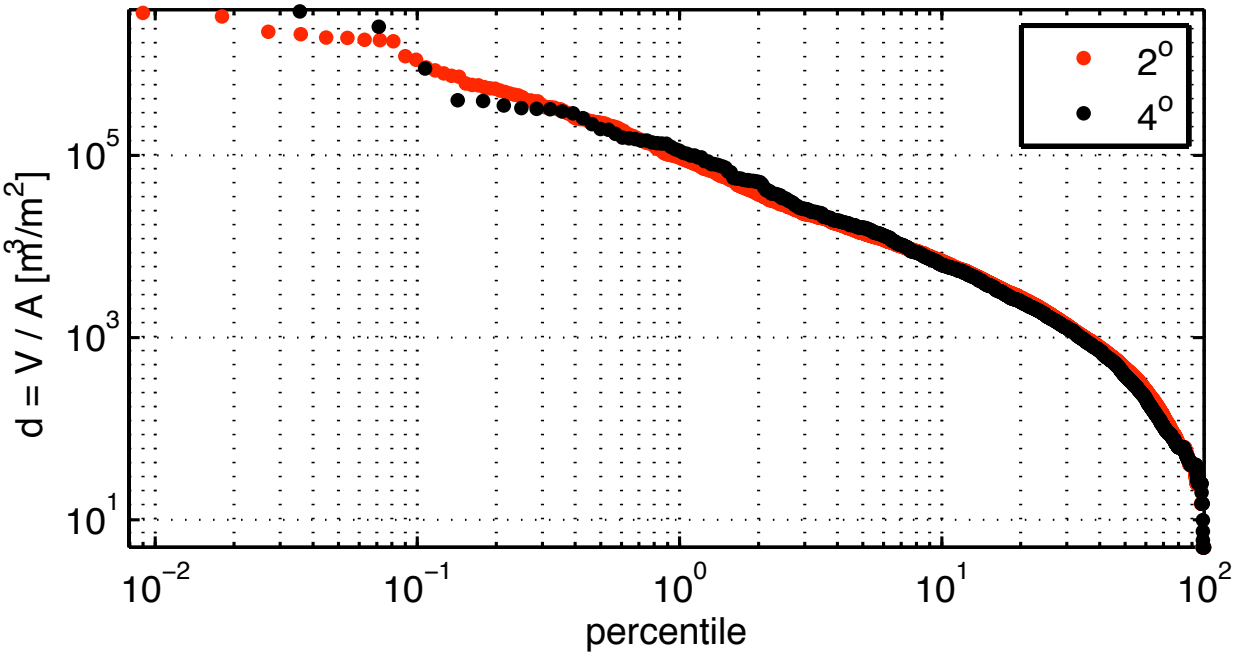

Figure 3. Comparing the distribution of water masses as calculated at 4° horizontal resolution (*black dots*) and as calculated at 2° resolution (*red dots*). The volume of the global ocean originating from each surface site is plotted in order of importance. The ranking of points is put into percentile to facilitate the comparison of the two resolutions.